ORIGINAL ARTICLE

Anodic Electrocatalysis of Glycerol Oxidation for Hybrid Alkali/Acid Electrolytic Hydrogen Generation

Xin Feng [a,b], Bo-Wen Liu [a], Ke-Xin Guo [a], Lin-Feng Fan [b], Gen-Xiang Wang [b], Su-Qin Ci [a,*], Zhen-Hai Wen [b,*]

[a] Key Laboratory of Jiangxi Province for Persistent Pollutants Control, National-Local Joint Engineering Research Center of Heavy Metals Pollutants Control and Resource Utilization and Resources Recycle, Nanchang Hangkong University, Nanchang, 330063, Jiangxi, China
[b] CAS Key Laboratory of Design and Assembly of Functional Nanostructures, and Fujian Key Laboratory of Nanomaterials, Fujian Institute of Research on the Structure of Matter, Chinese Academy of Sciences, Fuzhou, Fujian, 350002, China

Abstract

Electrolytic hydrogen production is heavily restricted by high-energy consumption majorly due to the relatively high potential of anodic oxygen evolution reaction (OER). Development of OER-alternative reaction at the anode has been recently proposed as a promising pathway to address the associated issues. In this work, we report a hybrid acid/alkali dual-electrolyte electrolyzer by coupling acidic hydrogen evolution reaction (HER) using commercial Pt/C cathode with alkaline electrocatalytic glycerol oxidation (GOR) which is implemented by developing a nickel foam (NF) supporting Co_3O_4 nanosheets anode that shows low overpotential and high selectivity toward GOR for formate production. The hybrid acid/alkali electrolyzer only requires an applied voltage of 0.55 V to achieve the electrolytic current density of 10 $mA \cdot cm^{-2}$ for glycerol conversion into formate at the anode and H_2 production at the cathode with the Faraday efficiency of about 100%. The present work may open a new avenue to maximize the electron utilization efficiency and implement the energy-saving green route for H_2 generation.

Keywords: Self-supporting electrode; Glycerol oxidation; Electrocatalysis; Acid/alkali dual-electrolyte electrolyzer; Hydrogen generation

1. Introduction

The development of green renewable energy to replace fossil fuel is imperative for humans due to the increasingly serious environmental pollution and energy crisis. Hydrogen has been considered an ideal energy carrier in the future thanks to its non-pollution, high energy density, and rich source [1,2]. However, the traditional methane reforming to produce hydrogen uses fossil fuels as energy, which is high energy consumed with releasing huge amount of CO_2 [3]. Hydrogen production by electrolysis of water is regarded as the most simple, efficient and green hydrogen production method, which can work in tandem with renewable electricity (e.g., solar, wind) for the future large-scale hydrogen production [4−6]. However, the sluggish kinetics and high overpotentials of anodic OER require a large amount of energy, severely limiting its development [7−10].

In addition, the low-value O_2 produced in the anode may mix with H_2 to form explosive H_2/O_2 gas. It has become an innovative strategy to improve the overall energy conversion efficiency of hydrochemical hydrogen production by replacing OER with electrooxidation reaction of the thermodynamically more favorable anodic reactions [11−15]. Electrocatalytic glycerol oxidation (GOR) theoretically requires a significantly lower theoretical oxidation potential (0.003 V *vs.* RHE) than OER

Received 1 June 2022; Received in revised form 23 June 2022; Accepted 29 August 2022
Available online 31 August 2022

* Corresponding author, Su-Qin Ci, Tel: (86-791) 83953378, E-mail address: sqci@nchu.edu.cn.
* Corresponding author, Zhen-Hai Wen, Tel: (86-591) 6317353, E-mail address: wen@fjirsm.ac.cn.

https://doi.org/10.13208/j.electrochem.2215005

(1.23 V *vs.* RHE). Moreover, glycerol, one of the main by-products of biodiesel production, is excess and cheap [16−18]. And glycerol can be converted into a variety of high value-added products, like dihydroxyacetone (DHA), glyceraldehyde (GALD), glyceric acid (GLA), formic acid, and other value-added products in the GOR process [19−24]. Therefore GOR instead of OER on the anode side could not only reduce the energy consumption of the electrolytic water hydrogen production system but also obtain liquid phase products and clean hydrogen with more added value than oxygen, realizing multiple benefits. Precious metals-based materials have been widely used as electrocatalysts for GOR, but the high cost and the scarcity of reservoirs hinder their practical application [25−27]. In recently, transition metal oxides/hydroxides, such as NiO, $Ni(OH)_2$, Co_3O_4, $Co(OH)_2$, CuO, and $Cu(OH)_2$, were reported to show decently high activity and selectivity for glycerol electrooxidation, which has attracted much attention due to low cost and low price [28−31]. However, the inherent low conductivity of naked transition metal oxides/hydroxides affect their practical application in GOR. Moreover, the concept of electrochemical neutralization energy (ENE) provides a new idea and method for the design and innovation of electrolytic cells in hydrolysis systems. By designing an acid-alkaline dual-electrolyte electrolyzer can provide a good pH environment for the anode GOR and cathode HER, respectively, which can not only reduce the required electrical energy but also promote the reaction kinetics [15,32−34].

Herein, we report a simple hydrothermal-calcination process for *in-situ* growth of Co_3O_4 nanosheets (Co_3O_4/NF) on NF substrates as an efficient electrocatalyst for GOR, which only requires 1.21 V *vs.* RHE to reach 10 $mA \cdot cm^{-2}$ and showing high selectivity with Faraday efficiency (FE) of over 85% in a wide potential (1.2−1.5 V *vs.* RHE) toward formate products.

Then, an acid-alkaline dual-electrolyte electrolyzer device was designed and assembled by paring Co_3O_4/NF as the anode of GOR in alkaline electrolyte with commercial Pt/C as the cathode of acid electrolyte. The electrolytic cell requires only a low applied voltage of 0.55 V to reach 10 $mA \cdot cm^{-2}$ and exhibits capability to produce H_2 and formate in high stability and a high FE.

2. Experimental section

2.1. Reagents and chemicals

Cobalt nitrate hexahydrate ($Co(NO_3)_2 \cdot 6H_2O$), methanol, ethanol, hydrochloric acid, and glycerol were purchased from Sinopharm Chemical Reagent Co., Ltd (Shanghai, China). 2-methylimidazole and Dimethyl sulfoxide (DMSO) were purchased from Shanghai Titan Technology Co., Ltd respectively. D_2O and Pt/C (20 wt.%) were bought from Macklin. All the deionized water used in the experiment was self-made in the laboratory. NF was purchased from Suzhou Taili Foam Metal Factory. All reagents are analytically pure and can be used without further purification.

2.2. Materials characterizations

X-ray diffraction (XRD) analysis of the sample structure and crystal morphology, X-ray diffractometer (Cu $K\alpha$) (D8ADVANCE-A25, Bruker, Germany). Scanning electron microscope (SEM) images were taken using a scanning electron microscope (Nova NanoSEM 450, FEI). Transmission electron microscope (TEM) and energy-dispersive X-ray spectroscopy (EDS) images were performed on Talos F200X (FEI, USA). Surface compositions of the catalysts were examined by X-ray photoelectron spectroscopy (XPS) (ESCALAB 250Xi, Thermo Scientific, USA). The products of glycerol oxidation were characterized by superconducting nuclear magnetic resonance spectroscopy (NMR) (AVANCE 400, Jobin Yvon, France).

2.3. Preparation of catalyst

The self-supporting Co_3O_4 nanosheets cathode material is grown *in situ* on NF by a simple hydrothermal-calcination method. First, 2×3 cm^2 NF was intercepted for pretreatment: NF was put into 3 $mol \cdot L^{-1}$ HCl, ethanol, and deionized water for ultrasonic treatment for 10 min, respectively, and dried for use. 2.91 g $Co(NO_3)_2 \cdot 6H_2O$ and 0.164 g 2-methylimidazole were dissolved in 20 mL methanol respectively, stirring for 30 min to form solution A and solution B. Solutions A and B were then mixed and stirred evenly to obtain solution C. Afterward, the solution C and treated NF were put into the stainless steel autoclave (lined with Teflon), after reaction at 140 °C for 12 h, cool naturally at room temperature, clean the sample surface with methanol and ethanol, and then dry it in a 60 °C vacuum drying oven for 12 h. Finally, put the sample into a tubular furnace and burn it at 350 °C (heating rate: 2 $°C \cdot min^{-1}$), and air atmosphere for 2 h to obtain Co_3O_4/NF catalyst.

2.4. Electrochemical characterization

To test the catalytic activity of the material, the electrochemical test was carried out in a three-electrode system using the CHI 760E electrochemical workstation (CH Instruments,

Shanghai, Chenhua Co., Ltd.). Co_3O_4/NF electrode (1 cm^{-2}) is directly used as the working electrode, carbon rod as the counter electrode, and Hg/HgO (1 $mol \cdot L^{-1}$ KOH) as the reference electrode. All potentials of electrochemical test refer to reversible hydrogen electrode (RHE)

$$E(\mathrm{RHE}) = E(\mathrm{Hg/HgO}) + 0.05916 \times \mathrm{pH} + 0.098$$

To eliminate the interference of oxygen with the test results, N_2 is introduced into the electrolyte for 30 min before the test. Prior to the electrochemical test, cyclic voltammetry (CV) measurements were performed several times until the cycle stabilized to activate the system. Linear sweep voltammetry (LSV) was carried out in 1 $mol \cdot L^{-1}$ KOH electrolyte at a scanning rate of 5 $mV \cdot s^{-1}$, with and without 0.5 $mol \cdot L^{-1}$ glycerol. Determination of electrochemical impedance spectroscopy (EIS), which is carried out in the frequency range of 0.1−10,000 Hz and amplitude of 5 mV. In the non-Faradaic reaction potential region, the electrochemical double-layer capacitance (C_{dl}) of the material in the potential region was confirmed by CV at different scanning speeds, and the electrochemical active area (ECSA) was calculated based on C_{dl} data.

2.5. Assembly and tests of the acid-alkaline dual-electrolyte electrolyzer

We have designed and Assembly an acid-alkaline dual-electrolyte electrolyzer based on ENE theory, in which Co_3O_4/NF is used as the anode in 1 $mol \cdot L^{-1}$ KOH solution containing 0.5 $mol \cdot L^{-1}$ glycerol and Pt/C as the cathode in 0.5 $mol \cdot L^{-1}$ H_2SO_4. A bipolar membrane (BPM) was used to separate the cathode chamber from the anode chamber in which glycerol is electrooxidized on the alkaline anode to produce electrons, the electrons are transferred to the acidic cathode through the external circuit, and the electrons obtained by H^+ are reduced to H_2, while K^+ enters the cathode chamber through the bipolar film, and SO_4^{2-} enters the anode chamber from the cathode chamber through the bipolar film to form a complete circuit. The hydrogen in the device was collected by drainage method, and the electrochemical test was carried out with a double electrode system on the CHI760E electrochemical workstation, and the products after anodic glycerol oxidation were tested and analyzed.

2.6. Product quantification

The electrolytes oxidized by anodic glycerol in the three-electrode system and double-electrode system were tested by NMR. For each NMR measurement, 2 mL electrolyte with addition of 400 μL D_2O and 3.4 μL DMSO as an internal standard were used to analyze the liquid products. The standard solutions of glycerol and HCOOK are also dissolved in 1 $mol \cdot L^{-1}$ KOH solution for nuclear magnetic resonance testing. The FE of formate in GOR can be calculated by the following Eq. (1), and the Faraday efficiency of hydrogen precipitation in HER can be calculated by the following Eq. (2) [15,32].

$$\mathrm{FE(formate)} = \frac{N(\mathrm{fomate})}{Q_1/(z_1 \times F)} \times 100\% \quad (1)$$

$$\mathrm{FE}(H_2) = \frac{N(H_2)}{Q_2/(z_2 \times F)} \times 100\% \quad (2)$$

where Q_1 and Q_2 are the total charges passed through the electrodes, $z_1 = 8/3$ is the number of electrons that form a mole of formate, $z_2 = 2$ is the number of electrons that produce a molecule of H_2, and F is the Faraday constant (96,485 $C \cdot mol^{-1}$).

3. Results and discussion

Noticing that cobalt-based oxides have good GOR properties, we have designed a process for *in-situ* growth of Co_3O_4 on NF as a self-supporting electrode (Co_3O_4/NF). The schematic synthesis process of Co_3O_4/NF is illustrated in Fig. 1a. Firstly, the precursors of Co-based oxides grown on NF were uniformly grown on the NF framework (Fig. 1c) by hydrothermal method, but only the pretreated NF showed a smooth metal surface (Fig. 1b). After calcination and annealing, the morphology of Co_3O_4/NF still appears as nanosheets grown on the surface of NF (Fig. 1d), but the nanosheets are more wrinkled and rougher than that before annealing. Co_3O_4 nanosheets are uniformly and densely distributed on the NF matrix. The high-resolution TEM image (Fig. 1e) shows clear lattice stripes with a lattice fringe spacing of 0.243 nm corresponding to the Co_3O_4 (311) plane. The elemental pattern (Fig. 1f) shows that Co and O elements are uniformly distributed in the nanosheets.

The crystal structure information of Co_3O_4/NF nanosheets was analyzed by XRD, as shown in Fig. 2a. Except for the diffraction peaks of nickel, the peaks at 19, 31.3, 36.9, 44.8, 59.4 and 65.3° belong to (111), (220), (311), (400), (511) of Co_3O_4 (PDF 42-1467), respectively and (440) planes. And the XRD pattern of the samples obtained by treating the remaining powder after the hydrothermal reaction with the same experimental method further proves that the *in situ* growth on

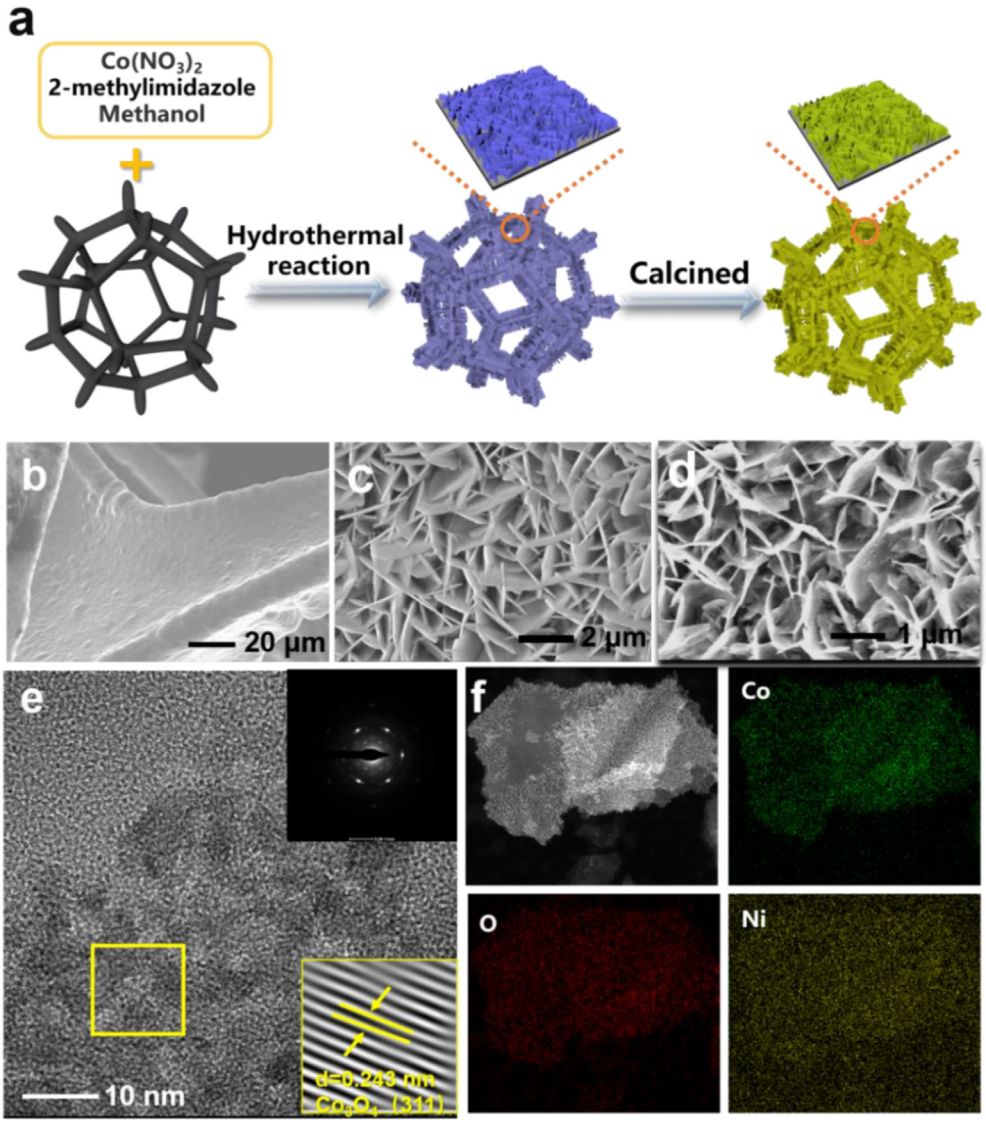

Fig. 1. (a) Scheme showing the synthesis strategy of Co_3O_4/NF (b) SEM of the NF. (c) SEM of the precursors of Co_3O_4/NF. (d) SEM of the Co_3O_4/NF. (e) HRTEM of the Co_3O_4/NF. (f) Corresponding element mappings of the Co_3O_4/NF nanosheets.

NF is Co_3O_4 nanosheets. In addition, the precursors of Co_3O_4/NF were also tested by XRD, and the results only showed a single peak of nickel (Fig. S1). The survey XPS spectrum in Fig. 2b confirmed the co-existence of Co, O elements on the surface of Co_3O_4/NF. The high-resolution XPS of Co 2p can be observed that the Co 2p region is two pairs of spin-orbit double star peaks and two pairs of related jitter satellite peaks (Fig. 2c). The bimodal Co $2p_{3/2}$ and Co $2p_{1/2}$ of the two pairs of spin orbits are Co^{3+} (779.3 eV and 794.6 eV) and Co^{2+} (780.7 eV and 795.9 eV), respectively, and the satellite peaks are (786.9 eV and 803.7 eV) and (788.2 eV and 805.2 eV) [35]. Fig. 2d shows the high-resolution XPS of O 1s, showing that the two characteristic peaks are 531.4 eV and 529.1 eV, respectively, in which the peak at 531.4 eV represents the defect oxygen with low oxygen coordination in the Co_3O_4 matrix, and the peak at 529.1 eV represents the lattice oxygen with low binding energy [35–37].

4. Electrocatalytic performance of GOR

The electrocatalytic properties of GOR were investigated at the set of electrodes in a three-electrode system (Fig. 3a–c). Fig. 3a shows the LSV curve of the Co_3O_4/NF electrode with and without 0.5 mol·L^{-1} glycerol in 1 mol·L^{-1} KOH solution. In the absence of 0.5 mol·L^{-1} glycerol in the electrolyte, the Co_3O_4/NF shows moderate OER activity with reaching a current density of 10 mA·cm^{-2} at 1.53 V *vs.* RHE, this potential value significantly decreases to 1.21 *vs.* RHE in 1.0 mol·L^{-1} KOH containing 0.5 mol·L^{-1} glycerol, indicating GOR is thermodynamically favorable

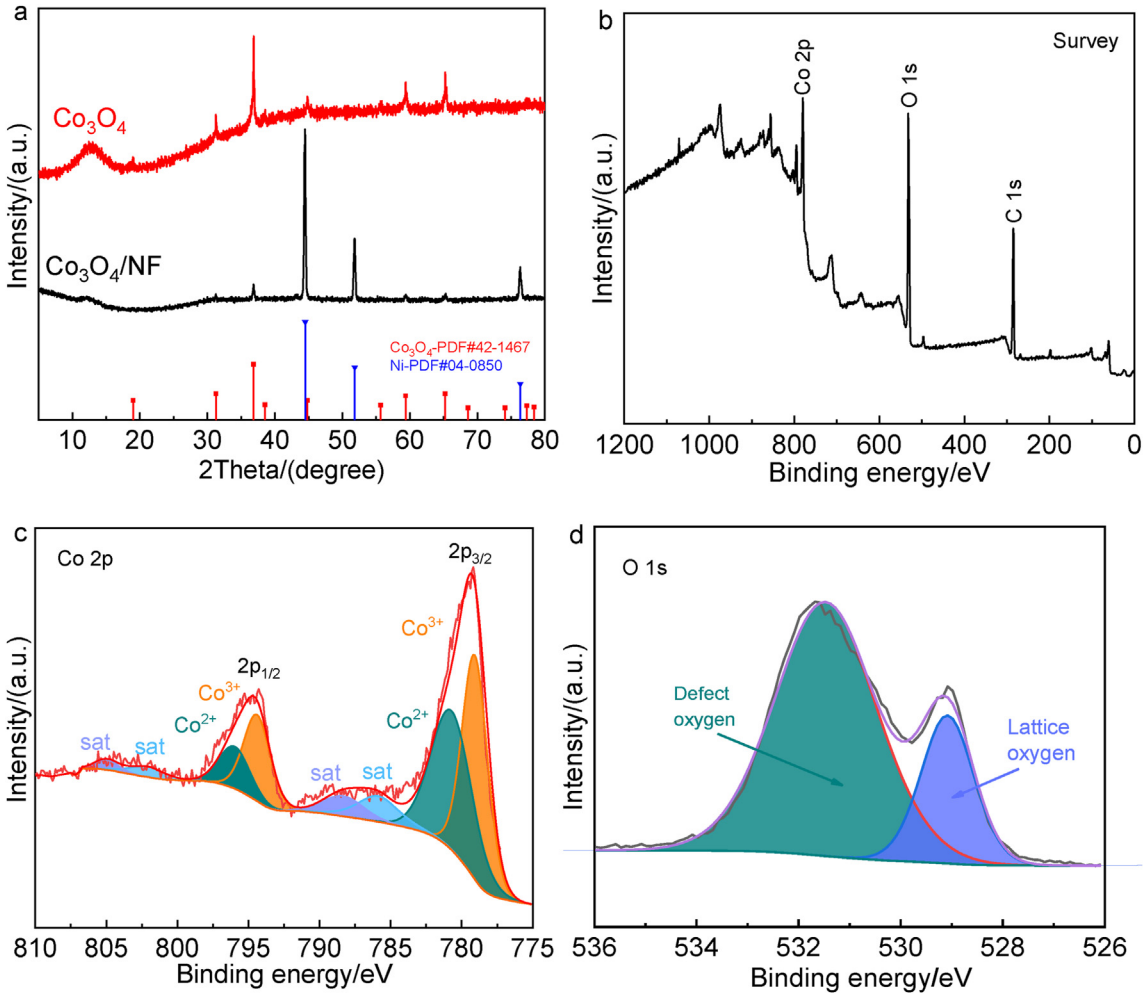

Fig. 2. (a) XRD pattern. (b) The survey XPS spectrum of Co_3O_4/NF. (c) High-resolution XPS spectra of Co 2p and (d) O 1s.

relative to OER on Co_3O_4/NF catalysts. To show the reaction potential of GOR and OER corresponding to 10 cm^{-2} and 100 cm^{-2} more clearly, Fig. 3b was drawn according to the LSV curve of Fig. 3a. Fig. 3b showed that the catalytic activity of the Co_3O_4/NF electrode was the highest when 0.5 $mol \cdot L^{-1}$ glycerol was added, and the catalytic initial potential changed to 1.21 V *vs.* RHE. In addition, we also compared the LSV curves of Co_3O_4/NF, precursors of Co_3O_4/NF, and NF after adding 0.5 $mol \cdot L^{-1}$ glycerol to 1 $mol \cdot L^{-1}$ KOH electrolyte (Fig. S2a). Co_3O_4/NF has the best catalytic performance. Fig. 3c shows the Tafel curve based on the LSV curve, which shows a lower Tafel slope of GOR (121.5 $mV \cdot dec^{-1}$) than that of OER (134.1 $mV \cdot dec^{-1}$), the results further illustrate that the catalytic kinetics of Co_3O_4/NF electrode in GOR is faster than that in OER. In addition, the effect of glycerol concentration in the electrolyte on the performance of glycerol in anodization was investigated, and the glycerol concentration was optimized, the catalyst was found to have the highest GOR activity in 1 $mol \cdot L^{-1}$ KOH containing 0.5 $mol \cdot L^{-1}$ glycerol (Fig. S2b). Moreover, the ECSA of the electrode was estimated by calculating the double-layer capacitance (C_{dl}) of the electrode through the cyclic voltammetry (CV) curve (Fig. S3). The C_{dl} value of Co_3O_4/NF (16.5 $mF \cdot cm^{-2}$) is significantly higher than that of Co_3O_4/NF precursor (11.3 $mF \cdot cm^{-2}$) and NF (0.3 $mF \cdot cm^{-2}$), indicating that Co_3O_4/NF has the largest ECSA and exposes more active sites. EIS results show that the Co_3O_4/NF electrode has a smaller charge transfer resistance than other electrodes (Fig. S4), indicating that the charge transfer rate is the fastest.

The GOR stability of Co_3O_4/NF was evaluated by chronopotentiometry (CP) technique at a fixed current density of 10 $mA \cdot cm^{-2}$, which shows after 12 h of continuous operation of the Co_3O_4/NF electrode, the potential did not increase significantly, and the LSV curve after the stability test only decreased slightly (Fig. S5). As shown in Fig. 3d, the reaction products were

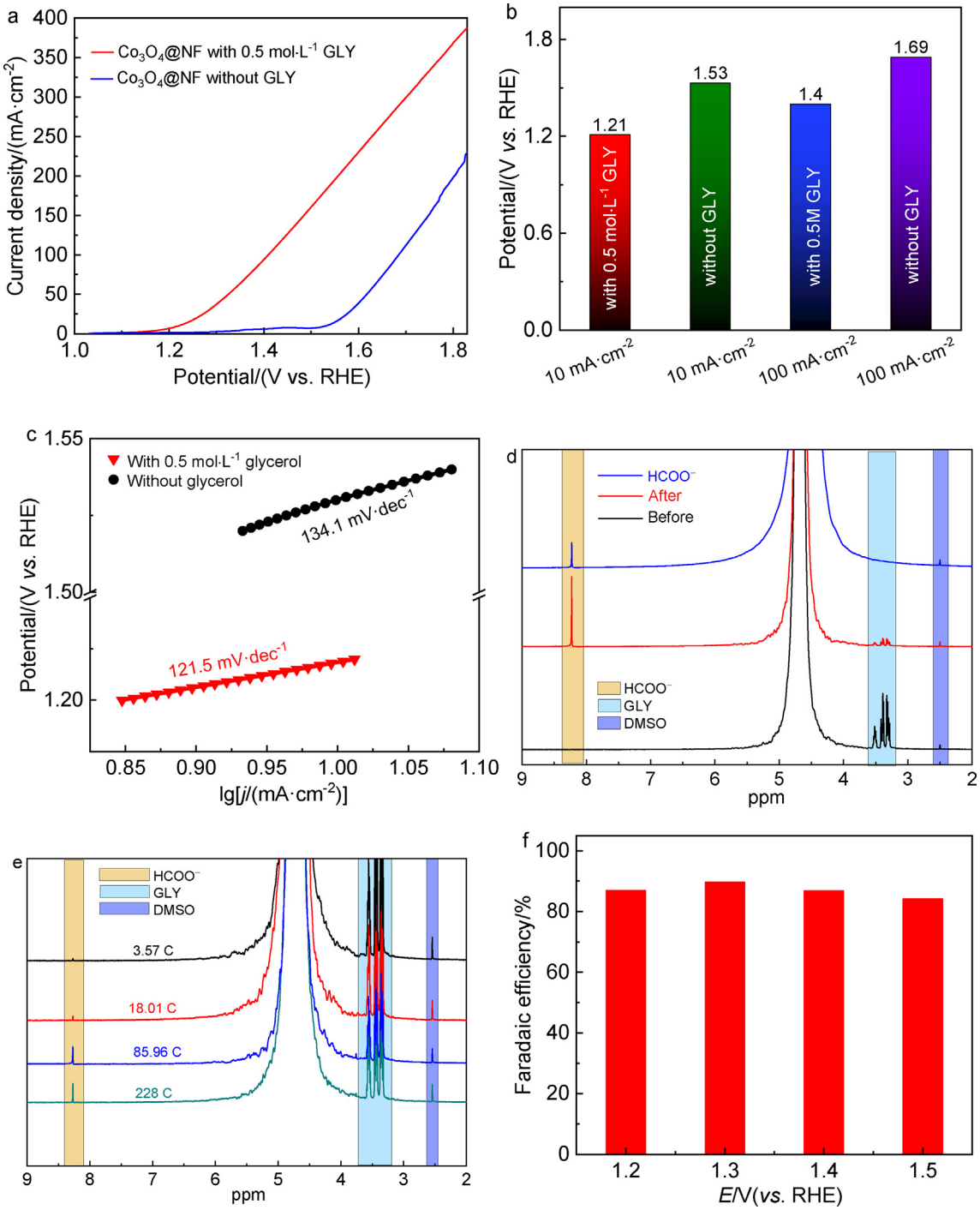

Fig. 3. (a) The LSV curve of electrocatalytic oxidation of Co_3O_4/NF electrode in 1 mol·L^{-1} KOH with or without 0.5 mol·L^{-1} glycerol added to the anode. (b) The potential corresponds to the LSV curve at 10 cm^{-2} and 100 cm^{-2}. (c) The Tafel curve corresponds to the LSV curve of whether or not 0.5 mol·L^{-1} glycerol is added to the 1 mol·L^{-1} KOH of the Co_3O_4/NF electrode. (d) Using DMSO as the internal standard (purple), the ^{1}H NMR spectra of the products before and after glycerol (blue) oxidation for 12 h on the Co_3O_4/NF electrode were determined. And the nuclear magnetic resonance spectrum of standard formate (yellow) proved that formate is the main product of glycerol oxidation. (e) Using DMSO as the internal standard to determine the ^{1}H NMR spectrum of oxidized glycerol under different charges. (f) FE produced for formate.

qualitatively and quantitatively analyzed by ^{1}H NMR, and the results showed that the anodic glycerol electrolysis product was only formate. Fig. 3e–f shows the Co_3O_4/NF electrode achieved a high selectivity to formate production with FE over 85% in a wide voltage range of 1.2–1.5 V vs. RHE, and the FE of formate reaches the highest at 1.3 V vs. RHE (89.7%). At the same time, may be due to the generation of some gas product (e.g., CO_2, O_2) in the

electrolysis process, resulting in the calculated formate FE of less than 100%.

Then, as shown in Fig. 4a and Fig. S6, an acid-alkaline dual-electrolyte electrolyzer was set up by using Co_3O_4/NF as the, in which Co_3O_4/NF is used as the anode with the electrolyte of 1 mol·L^{-1} KOH solution containing 0.5 mol·L^{-1} glycerol as the anolyte, pairing with Pt/C as the cathode in 0.5 mol·L^{-1} H_2SO_4. And a BPM was used to separate the cathode chamber from the anode chamber in which glycerol is electrooxidized on the alkaline anode to produce electrons, the electrons are transferred to the acidic cathode through the external circuit, and the electrons obtained by H^+ are reduced to H_2, while K^+ enters the cathode chamber through the bipolar film, and SO_4^{2-} enters the anode chamber from the cathode chamber through the bipolar film to form a complete circuit. As shown in Fig. 4b, when there is no glycerol in the anolyte, the pH gradient between the anodic (pH = 14) and cathodic (pH = 0) chambers can contribute a considerable voltage (0.059 × ΔpH) thanks to the electrochemical neutralization energy (ENE), acid-alkaline dual-electrolyte electrolyzer can deliver a current density of 10 mA·cm^{-2} at an applied voltage of 0.91 V, which is much lower than the theoretical voltage (1.23 V) for water electrolysis. As expected, with addition of 0.5 mol·L^{-1} glycerol into the anolyte, due to the thermodynamically favorable GOR over OER and the joint contribution of ENE, the applied voltage can be further reduced to 0.55 V to achieve an electrolytic current density of 10 mA·cm^{-2}, which is much lower than traditional alkaline electrolytic cell and those reported small-molecule oxidation-assisted water splitting (Table S1 and Fig. S7). At the same time, we also set up an acid-alkaline dual-electrolyte electrolyzer to test the bare NF as the anode of GOR, and the results further proved the modification and electrocatalytic effect of Co_3O_4 on NF (Fig. S8). Moreover, we compared the actual hydrogen production of HER in the acid-alkaline dual-electrolyte electrolyzer with the theoretical calculation, and the results showed that the measured hydrogen production was consistent with the theoretical one (Fig. S9).

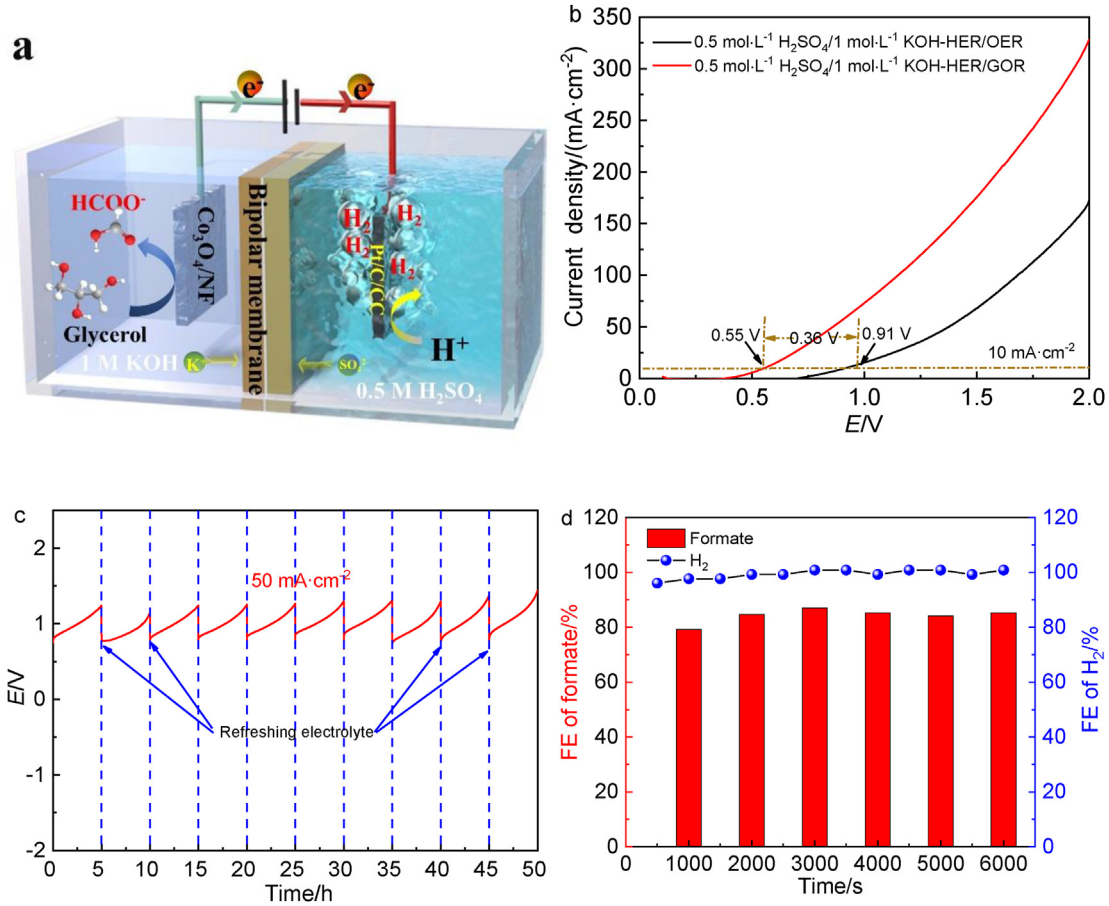

Fig. 4. (a) Schematic diagram of the Pt/C/CC || Co_3O_4/NF acid-alkaline dual-electrolyte electrolyzer. (b) Comparison of LSV curves of GOR and OER in the acid-alkaline dual-electrolyte electrolyzer. (c) Stability test of the acid-alkaline dual-electrolyte electrolyzer at a current density of 50 mA·cm^{-2}. (d) FEs of formate and H_2 in the acid-alkaline dual-electrolyte electrolyzer at 10 mA·cm^{-2}

As shown in Fig. 4c, the stability of the acid-alkaline dual-electrolyte electrolyzer is evaluated by CP at 50 $mA \cdot cm^{-2}$. The results showed that the cell could operate stably for 50 h with some potential fluctuations, which could be recovered by refreshing the electrolyte. The increase of potential required by electrolysis can be attributed to the consumption of H^+, OH^- and glycerol in the electrolyte. The potential required by electrolysis can be recovered by restoring the concentration of the electrolyte. The FE of hydrogen and formate in the acid-alkaline dual-electrolyte electrolyzer was tested by drainage method (Fig. S10) and ^1H NMR, respectively. As shown in Fig. 4d, only liquid formate product was detected in the anode electrolyte with the FE of around 87.02%, and the average FE (100%) of H_2 production is nearly consistent with those of theoretical ones. However, it is obvious that the variation of FE for H_2 generation. This may be because the process of H_2 generation was majorly due to the self-made drainage method. During the process of H_2 generation, the accumulation and release of hydrogen bubbles on the material surface will lead to changes and differences in readings and may cause errors. Therefore we will further improve the device in the follow-up work.

5. Conclusions

In summary, a self-supported electrode grown *in situ* on nickel foam by a simple hydrothermal-calcination method, which displayed high electrocatalytic performance for GOR in the alkaline electrolyte, capable of reaching a current density of 10 $mA \cdot cm^{-2}$ at 1.21 V *vs.* RHE and glycerol can be converted into formate under a wide potential window with a high FE (over 85%). And an acid-alkaline dual-electrolyte electrolyzer only demands an extremely low voltage of 0.55 V to reach the current density of 10 $mA \cdot cm^{-2}$ due to the ENE and glycerol oxidation, realizing the feasibility of energy-saving and efficient electrocatalytic glycerol value-added conversion auxiliary hydrogen evolution. This work not only provides ideas for the development and design of advanced electrocatalysts for glycerol oxidation but also provides a sustainable, low-cost, energy-efficient approach to develop routes for the production of value-added chemicals.

Acknowledgements

This work was financially supported by the National Natural Science Foundation of China (22168025), the Natural Science Foundation of Jiangxi Province (20192BAB203013, 20202ACBL203003), CAS-Commonwealth Scientific and Industrial Research Organization (CSIRO) Joint Research Projects (121835KYSB20200039), and the Joint Fund of the Yulin University and the Dalian National Laboratory for Clean Energy (Grant. YLU-DNL Fund 2021011).

References

[1] Rahman M Z, Kibria M G, Mullins C B. Metal-free photocatalysts for hydrogen evolution[J]. Chem. Soc. Rev., 2020, 49(6): 1887−1931.
[2] Li Z S, Li B L, Peng S H, Li D H, Yang S Y, Fang Y P. Novel visible light-induced g-C_3N_4 quantum dot/$BiPO_4$ nanocrystal composite photocatalysts for efficient degradation of methyl orange[J]. RSC Adv., 2014, 4(66): 35144−35148.
[3] Navarro R M, Pena M A, Fierro J LG. Hydrogen production reactions from carbon feedstocks: fossil fuels and biomass [J]. Chem. Rev., 2007, 107(10): 3952−3991.
[4] Li X M, Hao X G, Abudula A, Guan G Q. Nanostructured catalysts for electrochemical water splitting: current state and prospects[J]. J. Mater. Chem., 2016, 4(31): 11973−12000.
[5] He L Q, Zhang W B, Mo Q J, Huang W J, Yang L C, Gao Q S. Molybdenum carbide-oxide heterostructures: *In situ* surface reconfiguration toward efficient electrocatalytic hydrogen evolution[J]. Angew. Chem. Int. Ed., 2020, 59(9): 3544−3548.
[6] Zhu J, Hu L S, Zhao P X, Lee L YS, Wong K Y. Recent advances in electrocatalytic hydrogen evolution using nanoparticles[J]. Chem. Rev., 2020, 120(2): 851−918.
[7] Mallouk T E. Water electrolysis: divide and conquer[J]. Nat. Chem., 2013, 5(5): 362−363.
[8] Li X R, Wang C L, Xue H G, Pang H, Xu Q. Electrocatalysts optimized with nitrogen coordination for high-performance oxygen evolution reaction[J]. Coord. Chem. Rev., 2020, 422: 213468.
[9] Xu Q C, Jiang H, Duan X Z, Jiang Z, Hu Y J, Boettcher S W, Zhang W Y, Guo S J, Li C Z. Fluorination-enabled reconstruction of nife electrocatalysts for efficient water oxidation[J]. Nano Lett., 2021, 21(1): 492−499.
[10] Cao S S, Qi J D, Lei F C, Wei Z M, Lou S S, Yang X Y, Guo Y Q, Hao P, Xie J F, Tang B. Reduction-induced surface reconstruction to fabricate cobalt hydroxide/molybdenum oxide hybrid nanosheets for promoted oxygen evolution reaction[J]. Chem. Eng. J., 2021, 413: 127540.
[11] Lu S L, Zhao B, Chen M X, Wang L, Fu X Z, Luo J L. Electrolysis of waste water containing aniline to produce polyaniline and hydrogen with low energy consumption[J]. Int. J. Hydrogen Energy, 2020, 45(43): 22419−22426.
[12] Ding Y, Xue Q, Hong Q L, Li F M, Jiang Y C, Li S N, Chen Y. Hydrogen and potassium acetate Co-production from electrochemical reforming of ethanol at ultrathin cobalt sulfide nanosheets on nickel foam[J]. ACS Appl. Mater. Interfaces, 2021, 13(3): 4026−4033.
[13] Sun F C, Zhou Y, You Z H, Xia H H, Tuo Y X, Wang S T, Jia C P, Zhang J. Bi-functional Fe_3O_4/Au/CoFe-LDH sandwich-structured electrocatalyst for asymmetrical electrolyzer with low operation voltage[J]. Small 2021: e2103307.
[14] Duan Y J, Liu Z L, Zhao B, Liu J H. Raspberry-like Pd_3Pb alloy nanoparticles: superior electrocatalytic activity for ethylene glycol and glycerol oxidation[J]. RSC Adv., 2020, 10(27): 15769−15774.
[15] Zheng D D, Li J W, Ci S Q, Cai P W, Ding Y C, Zhang M T, Wen Z H. Three-birds-with-one-stone electrolysis for

energy-efficiency production of gluconate and hydrogen[J]. Appl. Catal., B, 2020, 277: 119178.

[16] Kim H J, Kim Y, Lee D E, Kim J R, Chae H J, Jeong S Y, Kim B S, Lee J, Huber G W, Byun J, Kim S, Han J. Co-producing value-added chemicals and hydrogen with electrocatalytic glycerol oxidation technology: experimental and techno-economic investigations[J]. ACS Sustain. Chem. Eng., 2017, 5(8): 6626−6634.

[17] Pagliaro M, Ciriminna R, Kimura H, Rossi M, Della Pina C. From glycerol to value-added products[J]. Angew. Chem. Int. Ed., 2007, 46(24): 4434−4440.

[18] Park Y J, Yang J W. Glycerol conversion to high-value chemicals: the implication of unnatural α-amino acid syntheses using natural resources[J]. Green Chem., 2019, 21(10): 2615−2620.

[19] Chen Y X, Lavacchi A, Miller H A, Bevilacqua M, Filippi J, Innocenti M, Marchionni A, Oberhauser W, Wang L, Vizza F. Nanotechnology makes biomass electrolysis more energy efficient than water electrolysis[J]. Nat. Commun., 2014, 5: 4036.

[20] Behr A, Eilting J, Irawadi K, Leschinski J, Lindner F. Improved utilisation of renewable resources: new important derivatives of glycerol[J]. Green Chem., 2008, 10(1): 13−30.

[21] Anitha M, Kamarudin S K, Kofli N T. The potential of glycerol as a value-added commodity[J]. Chem. Eng. J., 2016, 295: 119−130.

[22] Dodekatos G, Schünemann S, Tüysüz H. Recent advances in thermo-, photo-, and electrocatalytic glycerol oxidation [J]. ACS Catal., 2018, 8(7): 6301−6333.

[23] Bozell J J, Petersen G R. Technology development for the production of biobased products from biorefinery carbohydrates—the US Department of Energy's "Top 10" revisited[J]. Green Chem., 2010, 12(4): 539−554.

[24] Fan L F, Liu B W, Liu X, Senthilkumar N, Wang G X, Wen Z H. Recent progress in electrocatalytic glycerol oxidation[J]. Energy Technol., 2020, 9(2): 2000804.

[25] Huang L, Sun J Y, Cao S H, Zhan M, Ni Z R, Sun H J, Chen Z, Zhou Z Y, Sorte E G, Tong Y YJ, Sun S G. Combined EC-NMR and *in situ* FTIR spectroscopic studies of glycerol electrooxidation on Pt/C, PtRu/C, and PtRh/C[J]. ACS Catal., 2016, 6(11): 7686−7695.

[26] Liu Y F, Yu W J, Raciti D, Gracias D H, Wang C. Electrocatalytic oxidation of glycerol on platinum[J]. J. Phys. Chem. C, 2018, 123(1): 426−432.

[27] Lee S, Kim H J, Lim E J, Kim Y, Noh Y, Huber G W, Kim W B. Highly selective transformation of glycerol to dihydroxyacetone without using oxidants by a PtSb/C-catalyzed electrooxidation process[J]. Green Chem., 2016, 18(9): 2877−2887.

[28] Tang S S, Li X G, Courté M, Peng J J, Fichou D. Hierarchical $Cu(OH)_2$@$Co(OH)_2$Nanotrees for water oxidation electrolysis[J]. ChemCatChem, 2020, 12(16): 4038−4043.

[29] Lv J J, Wang L M, Li R S, Zhang K Y, Zhao D F, Li Y Q, Li X J, Huang X B, Wang G. Constructing a hetero-interface composed of oxygen vacancy-enriched Co_3O_4 and crystalline−amorphous NiFe-LDH for oxygen evolution reaction[J]. ACS Catal., 2021, 11(23): 14338−14351.

[30] Kou Y, Liu J, Li Y B, Qu S X, Ma C, Song Z S, Han X P, Deng Y D, Hu W B, Zhong C. Electrochemical oxidation of chlorine-doped $Co(OH)_2$ nanosheet arrays on carbon cloth as a bifunctional oxygen electrode[J]. ACS Appl. Mater. Interfaces, 2018, 10(1): 796−805.

[31] Ray C, Lee S C, Jin B J, Kundu A, Park J H, Jun S C. Conceptual design of three-dimensional CoN/Ni_3N-coupled nanograsses integrated on N-doped carbon to serve as efficient and robust water splitting electrocatalysts [J]. J. Mater. Chem., 2018, 6(10): 4466−4476.

[32] Fan L F, Ji Y X, Wang G X, Chen J X, Chen K, Liu X, Wen Z H. High entropy alloy electrocatalytic electrode toward alkaline glycerol valorization coupling with acidic hydrogen production[J]. J. Am. Chem. Soc., 2022, 144(16): 7224−7235.

[33] Ding Y C, Cai P W, Wen Z H. Electrochemical neutralization energy: from concept to devices[J]. Chem. Soc. Rev., 2021, 50(3): 1495−1511.

[34] Wang G X, Chen J X, Li K K, Huang J H, Huang Y C, Liu Y J, Hu X, Zhao B S, Yi L C, Jones T W, Wen Z H. Cost-effective and durable electrocatalysts for Co-electrolysis of CO_2 conversion and glycerol upgrading[J]. Nano Energy, 2022, 92: 106751.

[35] Xu Y, Liu M Y, Wang S Q, Ren K L, Wang M Z, Wang Z Q, Li X N, Wang L, Wang H J. Integrating electrocatalytic hydrogen generation with selective oxidation of glycerol to formate over bifunctional nitrogen-doped carbon coated nickel-molybdenum-nitrogen nanowire arrays[J]. Appl. Catal., B, 2021, 298: 120493.

[36] Vo T G, Ho P Y, Chiang C Y. Operando mechanistic studies of selective oxidation of glycerol to dihydroxyacetone over amorphous cobalt oxide[J]. Appl. Catal., B, 2022, 300: 120723.

[37] Xie Y A, Zhou Z Y, Yang N J, Zhao G H. An overall reaction integrated with highly selective oxidation of 5-hydroxymethylfurfural and efficient hydrogen evolution[J]. Adv. Funct. Mater., 2021, 31(34): 2102886.

基于阳极甘油氧化电催化的碱/酸混合电解制氢研究

冯　辛 [a,b]，刘博文 [a]，郭可鑫 [a]，范林丰 [b]，王根香 [b]，次素琴 [a,*]，温珍海 [b,*]

[a] 南昌航空大学，江西省持久性污染物控制与资源循环利用重点实验室，江西 南昌 330063
[b] 中国科学院福建物质结构研究所，中科院功能纳米结构设计与组装重点实验室，福建省纳米材料重点实验室，福建 福州，350002

摘要

耦合可再生电能的电解水制氢是一项极具前景的绿氢技术，该技术仍受限于阳极析氧反应（OER）动力学慢、过电位高等问题的限制。在阳极端采用热力学更容易的电氧化反应代替 OER，可大幅降低电耗并且在阳极端获得增值产物，是电解制氢的一种新策略。甘油作为生物柴油生产的主要副产品且产能过剩，其电催化氧化（GOR）理论电位比 OER 低。基于此，本研究工作报道了一种耦合酸性析氢反应（HER）与碱性 GOR 的混合酸/碱双电解液的制氢电解器，其以泡沫镍（NF）支撑 Co_3O_4 纳米片（NS）电极（Co_3O_4·NSs/NF）为阳极，商用碳载铂修饰碳布电极为阴极。在阳极端，Co_3O_4·NSs/NF 对 GOR 电催化表现出较低的过电位和转化为甲酸盐的高选择性。在该混合酸/碱双电解液电解槽中，仅仅需要额外施加 0.55 V 的外加电压，即可达到 10 mA·cm^{-2} 的产氢电解电流密度，并可以在阳极将甘油高选择性地转化为甲酸盐，其中产氢的法拉第效率接近 100%。本研究工作为电解制氢提供了一条节电、阳极增值转化的技术路线。

关键词：自支撑电极；甘油电氧化；电催化；酸/碱双电解液电解；制氢